One step continuous hydrothermal synthesis of very fine stabilized superparamagnetic nanoparticles of magnetite

Lionel Maurizi, Frederic Bouyer, Jérémy Paris, Frédéric Demoisson, Lucien Saviot, Nadine Millot

Journal Name

Dynamic Article Links ►

Cite this:

www.rsc.org/xxxxxx

ARTICLE TYPE

One step continuous hydrothermal synthesis of very fine stabilized superparamagnetic nanoparticles of magnetite

Lionel Maurizi, Frédéric Bouyer, Jérémy Paris, Frédéric Demoisson, Lucien Saviot and Nadine Millot

Received (in XXX, XXX) Xth XXXXXXXXX 20XX, Accepted Xth XXXXXXXXX 20XX

DOI: 10.1039/b000000x

Stable suspensions of citrated SPIO nanoparticles were synthesised in one step using a hydrothermal continuous process. Citrates control the crystallite size and the oxidation degree of metallic ions despite the very short reaction time (4s). Magnetite particles, $Fe_{2.94}O_4$, with an average size of 4 nm and good monodispersity were obtained.

Magnetic nanoparticles with spinel structure such as magnetite Fe_3O_4 have proven their interest in many fields such as electronic [1], catalysis [2] or nanomedicine. [3] These materials are commonly synthesized by batch coprecipitation of a 1:2 Fe^{2+}/Fe^{3+} molar ratio in basic conditions [4, 5] or by decomposition of organometallic precursors. [6]

One of the most interesting properties of iron oxide nanoparticles is superparamagnetism, phenomenon observed when crystallite size is smaller than about 20 nm. [7] These nano-objects are usually named SPIO (SuperParamagnetic Iron Oxide). They are interesting for biomedical applications, in particular for Magnetic Resonance Imaging and nanovectorization. The surface chemistry of these SPIOs should be modified to be stable in physiological conditions. Most of the time, electrostatic agents such as citric acid,[8] DMSA,[9] phosphonates [10] or steric agents like PEG [11] or dextran [12] are used.

In spite of an exponential increase of their demand due to the development of nano-bioapplications, synthesis and surface modification of nanoparticles are still carried out using batch processes. In this context, hydrothermal continuous process could be an alternative to allow a large-scale production. [13-14] Thanks to the very short reaction time in this approach (few seconds), inorganic nanoparticles were produced with a very narrow size distribution in a yield from 10 to 15 grams per hour [15-17]. Nevertheless, a remaining technical challenge was to obtain stable suspension during such a hydrothermal process.

In the present paper, we describe the obtention of colloidal suspensions of SPIO with this continuous process. We have chosen citric acid for its electrostatic and biocompatible properties and its low cost for industrial utilization. [18] Moreover, the chelating properties of the basic form (citrates) should control crystallite growth [19], and its well-known anti-oxidizing properties should control deviation from oxygen stoichiometry, δ.

The hydrothermal continuous process was described in detail elsewhere. [15, 20] Briefly, a Fe^{2+}/Fe^{3+} salt aqueous solution (8.10^{-3} M/16.10^{-3} M) and a NaOH aqueous solution (0.33 M) were introduced counter-currently with the preheated distilled water (373K) in the mixing zone of the patented reactor[20] at 423K, leading to rapid heating and subsequent coprecipitation reaction. The total flow rate was set up at 60 mL.min^{-1} in order to get a reaction time of 4s. The pressure was regulated at 25 MPa thanks to a back pressure regulator. At the exit of the reactor, the suspension was rapidly cooled at room temperature. In order to study the influence of citrates, various amounts of chelator were introduced in the metal salt solution (citrate:iron ions molar ratio = 1:20, 1:5 and 1:1). The suspensions were collected in a HNO_3 solution (10^{-3} M) to quench crystal growth and then dialyzed for 3 days against water. Parts of them were freeze-dried for subsequent characterizations.

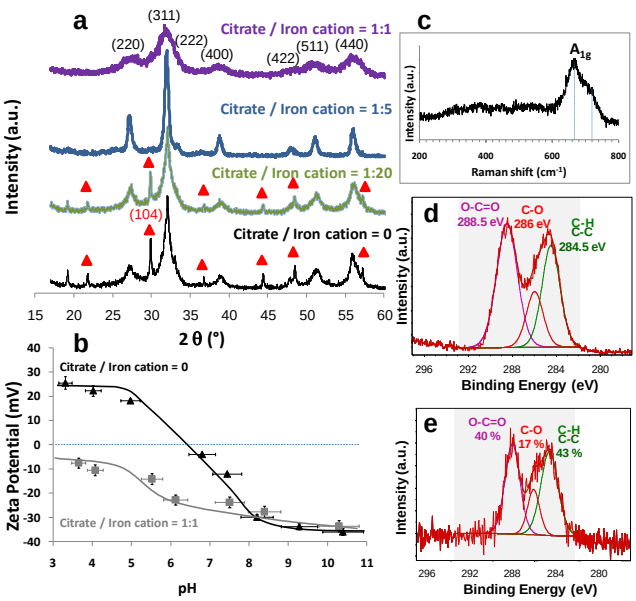

Fig. 1 (a) XRD pattern of iron oxide nanoparticles obtained by continuous hydrothermal synthesis and citrated with different ratios of citrate ions. The hematite phase is indexed by triangles; (b) Zeta potential curves of iron oxide nanoparticles without and with citrates (1:1); (c) Raman spectrum of citrated iron oxide nanoparticles (1:1). Carbon 1s level of pure citric acid (d) and of (1:1) citrated iron oxide nanoparticles (e).

Laboratoire Interdisciplinaire Carnot de Bourgogne, UMR 5209 CNRS-Université de Bourgogne, BP 47 870, F-21078 Dijon cedex, FRANCE. E-mail: nmillot@u-bourgogne.fr

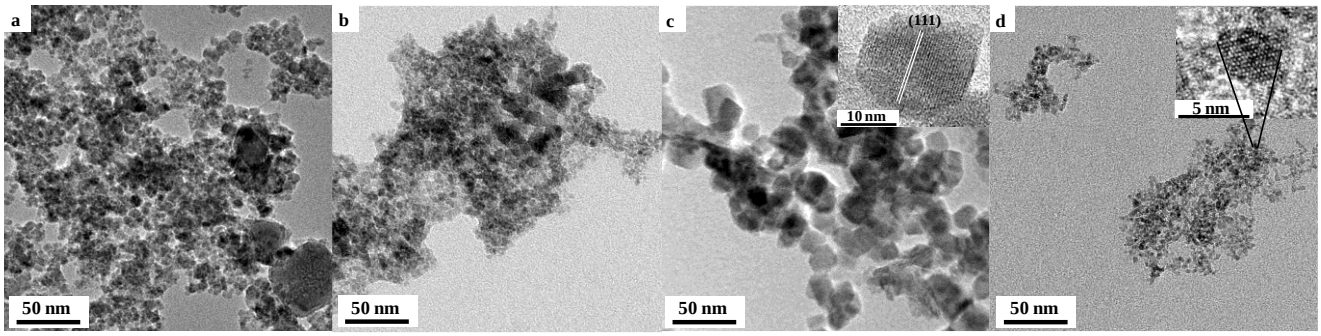

Fig. 2 Representative TEM images of iron oxide nanoparticles synthesized by continuous hydrothermal process in the presence of various citrate/iron cations molar ratios: a) absence of citrates ϕ_{TEM}=(9 ± 2) nm; b) 1:20 ϕ_{TEM}= (7 ± 2) nm; c) 1:5 ϕ_{TEM}= (21 ± 4) nm and d) 1:1 ϕ_{TEM}= (6 ± 2) nm. The mean sizes were obtained by counting at least a hundred of spinel crystallites. In inset HRTEM images.

The iron oxide nanoparticles obtained using this hydrothermal continuous process were mainly crystallized in the spinel phase (Fig. 1a). Nevertheless, without citrate ions, hematite phase appeared (indexed with triangles in Fig. 1a). The proportion of this undesired phase was approximately 12% in mass as obtained from the intensity ratio of the (104) peak of hematite to the (220) peak of magnetite. [21] With a 1:20 molar ratio of citrate/iron cations, the proportion of hematite was still of around 10%. However, with a molar ratio higher than 1:5 the hematite phase disappeared (Table 1).

Table 1 Structural parameters of iron oxide nanoparticles with different molar ratios of citrate ions.

Citrate/iron cation molar ratio	a (Å)	δ	Crystallite size[a] $Fe_{3(1-\delta)}O_4$ (nm)	Hematite (% in mass)	Crystallite size[a] α-Fe_2O_3 (nm)
0	8.371 ± 0.005	0.05	5.4 ± 0.1	12%	65 ± 1
1:20	8.366 ± 0.002	0.06	5.9 ± 0.1	10%	30 ± 2
1:5	8.396 ± 0.006	0	17.8 ± 0.4	n.d.[b]	-
1:1	8.389 ± 0.005	0.02	3.8 ± 0.1	n.d.[b]	-

[a] obtained by XRD pattern fitting. [b] n.d. not detected.

The crystallite sizes measured by XRD (Table 1) and confirmed by TEM (Figure 2) were influenced by the presence of citrate ions. Without citrates, the mean crystallite size of the spinel phase was around 5 nm and that of hematite phase 65 nm. With a 1:20 molar ratio, size of spinel phase was close to the previous one but hematite crystallite size decreased (from 65 to 30 nm). With citrate/iron cations ratio of 1:5 the mean crystallite size of magnetite was around 18 nm, and decreased to about 4 nm with a molar ratio of 1:1 (Table 1 and Figure 2). With classical hydrothermal synthesis of iron oxide nanoparticles at 523 K for 24 hours (batch process), the XRD cristalite size was around 39 nm [22]. This value is significantly higher than that obtained with the continuous hydrothermal synthesis process (Table 1).

The calculated lattice parameters of the iron oxide nanoparticles allow to determine their deviation from oxygen stoichiometry, δ, in the formula $Fe_{3(1-\delta)}O_4$. [4, 23] These parameters have to be compared to the maghemite (γ-Fe_2O_3, δ = 1/9) and magnetite (Fe_3O_4, δ = 0) ones, 8.346 Å (JCPDS file 39-1346) and 8.396 Å (JCPDS file 19-629), respectively. Without citrates or with a molar ratio of 1:20, lattice parameters are close (see Table 1) and lead to δ = 0.05 and δ = 0.06 respectively. These two phases are more oxidized than with higher citrate amount. Indeed, the lattice parameters with citrate/iron cations ratios of 1:5 and 1:1 are very close to that of magnetite and lead to δ = 0 and δ = 0.02 repectively (Table 1). Raman spectroscopy also allows to differentiate the two iron oxide phases. The spectrum of citrated iron oxide nanoparticles with the ratio (1:1) is displayed in Fig. 1c. It exhibits the characteristic bands of magnetite at 668 cm^{-1} assigned to the A_{1g} vibration, which can be easily distinguished from maghemite ones at 720 cm^{-1} (Fig 1c). [22] This latter contribution is slighly present and may comes from a very small quantity of maghemite, as observed by lattice parameter calculation (δ=0.02, Table 1) and should be localised as a very thin layer at the surface of the magnetite nanoparticles. [24]

The formation of the hematite phase for low citrates/iron cations ratios may be explained by the growth of a part of the spinel structured iron oxide in oxidative conditions. In accordance with anti-oxidizing properties of citrates, these results clearly show that adding citrates in large quantity to inorganic precursors prevented formation of hematite phase and decreased the oxidation degree of the spinel structure. Prevention of hematite formation thanks to adding of organic compounds with reactants has already been evidenced but only in batch hydrothermal synthesis by S. Takami *et al.* [25] In this paper, n-decanoic acid ($C_9H_{19}COOH$) and n-decylamine ($C_{10}H_{21}NH_2$) were mixed with Fe^{2+} precursor in a molar ratio of 1:4. The reaction occurred at 473K during 600 s. The authors demonstrated that n-decylamine can prevent hematite formation, as we observed in our case with citrate ions. In one step they synthesized and modified surface iron oxide nanoparticles with mean size between 21 to 28 nm that are far bigger than the cristallite sizes we obtained by continuous way in 4 s. Moreover, their suspensions were not stable at physiological pH.

Citrate ions are well known, in batch method, to allow the dispersion of aggregates of iron oxide nanoparticles leading to stable suspension at physiological pH by changing the surface charge. [18, 19] The electrokinetic properties of our iron oxide nanoparticles were investigated by Zeta potential measurements (Fig. 1b). In the presence of citrates (molar ratio 1:1), iron oxide nanoparticles were negatively charged (-30 mV) at physiological pH compared to uncoated nanoparticles (≈ 0 mV), and well dispersed in these conditions (Fig. 3a and 3b). The hydrodynamic size of such aggregates was (45 ± 10) nm and agreed with HRTEM counting (38 ± 15) nm. The suspension of the nanoparticles with the molar ratio 1:1 was stable for more than

6 months. The very short time of reaction in our process between iron oxide nanoparticles and citrates was sufficient to modify chemical properties of the surface of iron oxide nanoparticles. The absence of degradation of citrates was proven both by FTIR (results not shown) and XPS analysis for the molar ratio 1:1. The contamination carbon calibration was set to 284.5 eV. Pure citric acid was first analyzed alone (Fig. 1d). The data obtained (binding energy and full width at half maximum of the various components) were then used for the functionalized oxides. Thanks to desummation of XPS carbon peak (Fig. 1e), the presence of citrates was demonstrated (carbon contributions of COOH, CH_2 and COH: close to theorical ones in pure citric acid). In our case, it is clear that a 1:20 molar ratio is not sufficient for any modification. This result could be explained by the low residence time in the reactor of the starting materials before being collected in the HNO_3 solution or by degradation of the small amount of citrates (not detected by XPS for the lowest ratios). When a 1:1 ratio is used, the chelating effect of citrate ions is predominant, preventing both oxidation and crystallite growth. It is noteworthy that modification of the surface of nanoparticles (water adsorption, oxydation) may lead to structural variations of the core of the nanoparticles. [4, 26] Citrates bound to the iron oxide surface may also lead to spinel stabilisation.

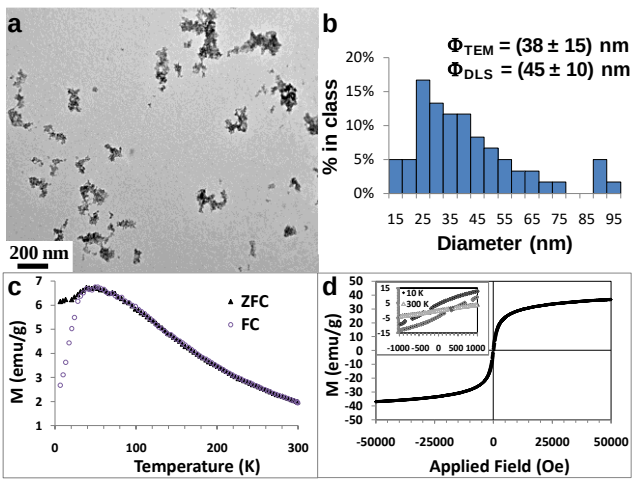

Fig. 3 Iron oxide nanoparticles obtained with a citrate ratio (1:1): (a) TEM picture and (b) counting of aggregates. (c) FC and ZFC curves under a field of 500 Oe. (d) Magnetization curve at 10 K, in inset hysteresis loop at 10K and 300K.

The thermal relaxation of the (1:1) citrated nanoparticles was probed by ZFC/FC measurements (Fig. 3c). The nanoparticles exhibit a superparamagnetic blocking temperature of 50 K at 500 Oe. Moreover, the peak in M(T) was broad, indicating a gradual transition to the superparamagnetic state. This may suggest both strong magnetic interactions beetween particles and a granulometric distribution.[27] The superparamagnetic state at ambiant temperature is also proven by hysteresis loops (insert Fig. 3d). The saturation magnetization of (1:1) citrated nanoparticles is 37 emu/g at 10 K (Fig. 3d). This value is lower than the theoretical value of the bulk magnetite (92 emu/g). It is usually attributed to the surface contribution: spin canting, surface disorder, adsorbed species (here principally citrates)…[22]

In conclusion, stoichiometric magnetite with particles of about 4 nm have been synthesised. For the first time, dispersing effects combined to the control of crystallite growth and prevention of Fe^{2+} oxidation thanks to surface modification *via* citrate ions have been described using hydrothermal continuous conditions. The obtained nanoparticles were superparamagnetic and dispersed in aggregates of 40 nm of mean diameter, and aqueous suspensions are stable more than 6 months at physiological pH. Those results open the way to continuous production on a large scale of stable SPIOs targeted for biomedical applications.

This work was supported by the Conseil Régional de Bourgogne. We would like to thank Dr R. Chassagnon for HRTEM images, M. Ariane for his help during hydrothermal synthesis, Dr O. Heintz for XPS analysis, Dr. E. Popova and Dr. Y. Dumont (from GEMaC and *via* the contract C'Nano IdF #IF-08-1453/R) for magnetic measurements.

Notes and references

1. S. K. Lim, K. J. Chung, Y. H. Kim, C. K. Kim and C. S. Yoon, *J. Colloid Interface Sci.*, 2004, **273**, 517-522.
2. G. P. Van der Laan and A. Beenackers, *Cat. Rev. - Sci. Eng.*, 1999, **41**, 255-318.
3. E. Duguet, S. Vasseur, S. Mornet and J. M. Devoisselle, *Nanomedicine*, 2006, **1**, 157-168.
4. T. Belin, N. Millot, F. Villieras, O. Bertrand, J.P. Bellat, *J. Phys. Chem. B*, 2004, **108**, 5333-5340.
5. R. Massart, E. Dubois, V. Cabuil and E. Hasmonay, *J. Magn. Magn. Mater.*, 1995, **149**, 1-5.
6. T. Hyeon, *Chem. Commun.*, 2003, 927-934.
7. J. L. Dormann, D. Fiorani and E. Tronc, *Adv. Chem. Phys.*, 1997, **98**, 283-494.
8. A. Hajdu, E. Illes, E. Tombacz and I. Borbath, *Colloids Surf. Physicochem. Eng. Aspects*, 2009, **347**, 104-108.
9. F. Bertorelle, C. Wilhelm, J. Roger, F. Gazeau, C. Menager and V. Cabuil, *Langmuir*, 2006, **22**, 5385-5391.
10. B. Basly, D. Felder-Flesch, P. Perriat, C. Billotey, J. Taleb, G. Pourroy and S. Begin-Colin, *Chem. Commun.*, 2010, **46**, 985-987.
11. L. Maurizi, H. Bisht, F. Bouyer and N. Millot, *Langmuir*, 2009, **25**, 8857-8859.
12. S. Mornet, J. Portier and E. Duguet, *J. Magn. Magn. Mater.*, 2005, **293**, 127-134.
13. T. Adschiri, K. Kanazawa and K. Arai, *J. Am. Ceram. Soc.*, 1992, **75**, 1019-1022.
14. A. Cabanas and M. Poliakoff, *J. Mater. Chem.*, 2001, **11**, 1408-1416.
15. N. Millot, B. Xin, C. Pighini and D. Aymes, *J. Eur. Ceram. Soc.*, 2005, **25**, 2013-2016.
16. N. Millot, S. Le Gallet, D. Aymes, F. Bernard and Y. Grin, *J. Eur. Ceram. Soc.*, 2007, **27**, 921-926.
17. A. Aimable, B. Xin, N. Millot and D. Aymes, *J. Solid State Chem.*, 2008, **181**, 183-189.
18. M. Racuciu, D. E. Creanga and A. Airinei, *Eur. Phy. J. E*, 2006, **21**, 117-121.
19. A. Bee, R. Massart and S. Neveu, *J. Magn. Magn. Mater.*, 1995, **149**, 6-9.
20. Demoisson, WO 2011010056 A1, 2011.
21. T. Belin, N. Millot, N. Bovet and M. Gailhanou, *J. Solid State Chem.*, 2007, **180**, 2377-2385.
22. T. J. Daou, G. Pourroy, S. Begin-Colin, J. M. Greneche, C. Ulhaq-Bouillet, P. Legare, P. Bernhardt, C. Leuvrey and G. Rogez, *Chem. Mater.*, 2006, **18**, 4399-4404.
23. P. Poix, *Bull. Soc. Chim. Fr.*, 1965, 1085-1087.
24. N. Guigue-Millot, Y. Champion, M.J. Hÿtch, F. Bernard, S. Bégin-Colin, P. Perriat, *J. Phys. Chem. B*, 2001, **105** (29), 7125-7132.
25. S. Takami, T. Sato, T. Mousavand, S. Ohara, M. Umetsu and T. Adschiri, *Materials Letters*, 2007, **61**, 4769-4772.
26. Y. Champion, F. Bernard, N. Guigue-Millot and P. Perriat, *Mater. Sci. Eng., A*, 2003, **360**, 258-263.
27. D. W. Kavich, S. A. Hasan, S. V. Mahajan, J.-H. Park, J. H. Dickerson, *Nanoscale Res Lett*, 2010, **5**, 1540–1545.